CD44 Promotes PD-L1 Expression and Its Tumor-Intrinsic Function in Breast and Lung Cancers

Tim Kong[1,2], Ryuhjin Ahn[3,4], Kangning Yang[1,2], Xianbing Zhu[1,2], Zheng Fu[1,2], Geneviève Morin[1,2], Rachel Bramley[1,2], Nikki C. Cliffe[1,2], Yibo Xue[1,2], Hellen Kuasne[1,2], Qinghao Li[1,2], Sungmi Jung[5], Anne V. Gonzalez[6], Sophie Camilleri-Broet[5], Marie-Christine Guiot[7], Morag Park[1,2], Josie Ursini-Siegel[1,3,4,8], and Sidong Huang[1,2]

ABSTRACT

The PD-L1 (CD274) immune-checkpoint ligand is often upregulated in cancers to inhibit T cells and elicit immunosuppression. Independent of this activity, PD-L1 has recently been shown to also exert a cancer cell–intrinsic function promoting tumorigenesis. Here, we establish this tumor-intrinsic role of PD-L1 in triple-negative breast cancer (TNBC) and non–small cell lung cancer (NSCLC). Using FACS-assisted shRNA screens, we identified the cell-surface adhesion receptor CD44 as a key positive regulator of PD-L1 expression in these cancers. Mechanistically, CD44 activated *PD-L1* transcription in part through its cleaved intracytoplasmic domain (ICD), which bound to a regulatory region of the *PD-L1* locus containing a consensus CD44-ICD binding site. Supporting this genetic interaction, CD44 positively correlated with PD-L1 expression at the mRNA and protein levels in primary tumor samples of TNBC and NSCLC patients. These data provide a novel basis for CD44 as a critical therapeutic target to suppress PD-L1 tumor–intrinsic function.

Significance: CD44 is a potential target to suppress PD-L1 function in TNBC. This finding has the potential to open a new area of therapy for TNBC.

Introduction

Programmed death-ligand 1 (PD-L1), also known as CD274, is a transmembrane protein that binds to the inhibitory receptor PD-1 on T cells and elicits T-cell anergy, leading to immune suppression (1). Many cancer cells upregulate PD-L1 surface expression to escape immune surveillance (2, 3). Neutralizing antibodies targeting PD-L1 or PD-1 can block T-cell anergy and resensitize tumor cells to antitumor immunity (3). These immune-checkpoint inhibitors are being intensively evaluated to treat poor-outcome cancers and have shown remarkable success in subsets of melanoma and lung cancer patients (3). Thus, understanding the regulation of cancer cell PD-L1 expression is essential to help devise treatment strategies to enhance cancer immunotherapy.

Triple-negative breast cancer (TNBC) is an aggressive subtype lacking effective treatment options. Unlike other subtypes, TNBCs do not express the estrogen receptor, progesterone receptor, and lack overexpression/amplification of HER2 (4). Therefore, chemotherapy remains the standard of care for this subtype, although only with an $\sim$ 20% response rate (5). Immune-checkpoint inhibitors are emerging as an attractive treatment option for TNBCs; however, they have only shown promising activities in a small subset of patients (3). Fewer than 20% of TNBCs respond to PD-1/PD-L1 checkpoint blockade therapy, and treatment combining an anti–PD-L1 antibody with paclitaxel chemotherapy minimally affected progression-free survival in metastatic TNBC patients (6, 7).

Recent studies suggest that although stromal PD-L1 is predictive of good outcome and increased response to PD-1 blockade, elevated PD-L1 levels in the tumor epithelium may paradoxically be associated with inferior outcome in TNBC patients (8–10). In addition, chemotherapy has recently been shown to significantly increase PD-L1 expression levels on TNBC cells and many TNBCs often themselves upregulate PD-L1 (11). These observations highlight an underappreciated role for tumor cell–intrinsic PD-L1 in increasing the tumorigenic potential of TNBCs independently of its immunosuppressive properties. Several studies have shown a role for tumor-intrinsic PD-L1 in controlling glucose metabolism in sarcomas and regulating cell growth and autophagy in ovarian cancer, melanoma, and prostate cancer, in which PD-L1 inhibition suppressed PI3K/AKT/mTOR signaling (12–14). However, the tumor-intrinsic functions of PD-L1 in TNBC have not been defined.

Similar to TNBC, non–small cell lung cancers (NSCLC) also express high levels of PD-L1. Although NSCLCs with *KRAS*-activating mutations show a trend toward higher PD-L1 expression (15–17), the association of *EGFR*-activating mutations and PD-L1 expression remains controversial between different studies (18, 19). Although a study showed that EGFR inhibition leads to decreased surface PD-L1

[1]Department of Biochemistry, McGill University, Montreal, Quebec, Canada. [2]Goodman Cancer Research Centre, McGill University, Montreal, Quebec, Canada. [3]Lady Davis Institute for Medical Research, Montréal, Quebec, Canada. [4]Department of Experimental Medicine, McGill University, Montréal, Quebec, Canada. [5]Department of Pathology, Glen Site, McGill University Health Centre Montreal, Quebec, Canada. [6]Department of Medicine, Division of Respiratory Medicine, McGill University Health Centre, Montreal Chest Institute, Montreal, Quebec, Canada. [7]Departments of Pathology, Montreal Neurological Hospital/Institute, McGill University Health Centre, Montreal, Quebec, Canada. [8]Department of Oncology, McGill University, Montréal, Quebec, Canada.

Note: Supplementary data for this article are available at Cancer Research Online (http://cancerres.aacrjournals.org/).

Corresponding Authors: Sidong Huang, McGill University, McIntyre Medical Building, Room 800, 3655 Promenade Sir William Osler, Montreal, Quebec H3G 1Y6, Canada. Phone: 514-398-4447; E-mail: sidong.huang@mcgill.ca; and Josie Ursini-Siegel, Departments of Oncology and Biochemistry, McGill University, 3755 Cote Ste. Catherine Road, Room# F528.1, Montreal, Quebec, Canada, H3T 1E2. Phone: 514-340-8222 × 6557; E-mail: giuseppina.ursini-siegel@mcgill.ca

Cancer Res 2020;80:444–57

doi: 10.1158/0008-5472.CAN-19-1108

expression in *EGFR*-mutant NSCLC cell lines (2), the cancer cell–intrinsic function of PD-L1 remains to be better established.

In addition to EGFR, the downstream AKT and ERK signaling pathways have also been implicated in the regulation of PD-L1 expression in breast cancer, NSCLC, and melanoma (2, 20–22). Furthermore, transcription factors such as STAT1, STAT3, NF-κB, and HIF-1α are known to activate *PD-L1* expression in response to inflammatory and metabolic cues from the tumor microenvironment (23–26). Besides these transcriptional regulators, CKLF Like MARVEL Transmembrane Domain Containing (CMTM) 4 and 6 have been shown to regulate PD-L1 protein stability (27, 28). Moreover, glycosylation and palmitoylation regulation of PD-L1 are important for its protein stabilization and PD-L1/PD-1 interaction (29, 30). Consistently, a monoclonal antibody targeting glycosylated PD-L1 has been shown to promote PD-L1 internalization and degradation in TNBC models (31). These studies highlight the importance of understanding how PD-L1 expression and activity are regulated in tumor cells.

In this study, we examined the cell-intrinsic function of PD-L1 in TNBC and NSCLC and investigated novel regulators of PD-L1 expression in these cancers using an unbiased functional genetic approach.

Materials and Methods

Cell culture and viral transduction

All cancer cell lines were obtained from the ATCC. CAMA-1, MCF-7, BT-474, SK-BR-3, MDA-MB-436, and Hs578T were cultured in Dulbecco's Modified Eagle Medium (Gibco) with 6% fetal bovine serum (FBS), 1% penicillin–streptomycin antibiotics, and 2 mmol/L L-glutamine. HCC1937, MDA-MB-231, BT-549, H1703, H838, EBC-1, HCC827, PC9, H358, A549, H23, and H1915 were cultured in RPMI-1640 (Gibco) with 6% FBS, 1% penicillin–streptomycin antibiotics, and 2 mmol/L L-glutamine. All cell lines were maintained at 37°C and 5% CO_2 and regularly tested for *Mycoplasma*. Identity of cell lines was verified by short tandem repeat profiling. From thawing, cells recovered for 2 passages and were passaged maximum 10 times when experiments were performed.

Lentiviral transduction was used to infect cells and performed using the protocol as described at http://www.broadinstitute.org/rnai/public/resources/protocols. Low multiplicity of infection (MOI) was used as high MOI in some cell lines resulted in elevated basal PD-L1 expression in control cells. Transduced cells were selected in puromycin or blasticidin for 2 to 4 days and plated for further assays immediately after selection.

Compounds and antibodies

Torin (S2827), MK-2206 (S1078), and trametinib (GSK1120212; S2673) were from Selleck Chemicals. Low-molecular-weight hyaluronan (GLR001) was from R&D Systems. Primary antibodies for PD-L1 (E1L3N), Phospho-AKT (Ser473; D9E), AKT (40D4), Phospho-S6 Ribosomal Protein (Ser235/236; D57.2.2E), and S6 Ribosomal Protein (54D2) were from Cell Signaling Technology; HSP90 (H-114), HSP90 (F-8), pERK (E-4), ERK 1 (C-16), ERK 2 (C-14), and HCAM (DF1485) were from Santa Cruz Biotechnology; primary antibodies against CREB1 (ab31387 and ab178322) and the intracellular domain of CD44 (ab24504) were from Abcam. Anti-V5 (R96025) was from Thermo Fisher Scientific.

Plasmids

Individual shRNA and ORF vectors used were from the Mission TRC library (Sigma), and ORF collections were developed by members of the ORFeome Collaboration (Sigma/TransOMIC), provided by Genetic Perturbation Service of Goodman Cancer Research Centre at McGill University: pLKO.5, sh*PD-L1*#1 (TRCN0000056916), sh*PD-L1*#2 (TRCN0000423296), sh*CD44*#1 (TRCN0000057564), sh*CD44*#2 (TRCN0000057566), sh*CD44*#3 (TRCN0000296191), sh*CREB*#1 (TRCN0000226467), sh*CREB*#2 (TRCN0000226468), pLX304-*eGFP,* pLX304-*PD-L1* (ccsbBroad304_03086), pLX304-*CD44* (ccsbBroad304_05963), pLX317-*eGFP,* pLX317-*PD-L1* (TRCN0000488557), and pLX317-*CREB1* (TRCN0000475150).

For the CD44-ICD expression construct, DNA oligonucleotides coding for the intracellular region of CD44 were synthesized by IDTDNA. NheI and EcoRI restriction sites were introduced flanking the protein-coding sequence of CD44-ICD, and a Kozak consensus sequence was inserted after the NheI cut site before an AUG start codon sequence. Synthesized and sequenced verified construct were then subcloned into the pPrime-CMV-GFP-PGK-Puro vector.

Protein lysate preparation and immunoblots

1×10^5 to 5×10^5 cells/well were seeded into 6-well or 12-well plates. After 24 to 48 hours, cells were washed with ice-cold PBS and lysed with protein sample buffer. Samples were processed with NuPAGE Novex Gel Electrophoresis Systems (Invitrogen) followed by standard Western blotting procedure.

RNA isolation and qRT-PCR

Seeded cells were collected with TRIzol (Invitrogen) for RNA isolation. cDNA was synthesized using the Maxima First-Strand cDNA Synthesis Kit (Thermo Fisher Scientific). Relative mRNA levels were measured through qRT-PCR using SYBR Green Master Mix (Roche) and normalized to the expression of β-actin (*ACTB*). Primer sequences are as follows:

ACTB forward, 5′-GTTGTCGACGACGAGCG-3′
ACTB reverse, 5′-GCACAGAGCCTCGCCTT-3′
PD-L1 forward, 5′-ACAGCTGAATTGGTCATCCC-3′
PD-L1 reverse, 5′-TGTCAGTGCTACACCAAGGC-3′
CD44 forward, 5′-CACGTGGAATACACCTGCAA-3′
CD44 reverse, 5′-GACAAGTTTTGGTGGCACG-3′

Short-term growth and cell viability assays

Single-cell suspensions were seeded at a density of 1×10^3 to 5×10^3 cells/well depending on cell size and proliferation into 96-well plates after selection. Cells were incubated for 1 to 4 days while being photographed by IncuCyte Zoom Live-Cell Analysis System. For cell viability assays, CellTiter-Blue (Promega) was used at growth endpoint.

Long-term colony formation growth assays

Single-cell suspensions were seeded at a density of 5×10^3 to 20×10^3 cells/well depending on cell size and proliferation rate into 6-well plates. After 7 to 14 days of culturing, cells were fixed with 4% formalin and stained with 0.1% w/v crystal violet before being photographed.

Apoptosis detection assays

Single-cell suspensions were seeded at a density of 5×10^2 to 10×10^2 cells/well into 96-well plates. Twenty-four hours after seeding, Annexin V apoptosis reagent (1:400 dilution; Essen Bioscience; 4641) or Caspase-3/7 apoptosis assay reagent (1:1,000 dilution; Essen

Bioscience; 4440) were added to the cells for 24 to 72 hours. IncuCyte Zoom Live-Cell Analysis System was used to measure cell confluency, and Annexin V and Caspase-3/7 signals. Apoptotic signals were normalized to cell confluency.

Drug treatment assays

1×10^5 to 3×10^5 cells were seeded into a 6-well plate and treated with MK-2206, trametinib, torin, and/or hyaluronic acid 24 hours after seeding. Lysates were collected after indicated duration post drug treatment. For long-term colony formation assays, drugs were refreshed every 3 days.

In vivo MDA-MB-231 mouse xenografts

All animal procedures (Animal Use Protocol) were approved by the Institutional Animal Care Committee according to guidelines defined by the Canadian Council of Animal Care and were conducted at the Lady Davis Institute for Medical Research.

Doxycycline-inducible PD-L1 knockdown

MDA-MB-231 cells were infected with tet-on pLKO-5 (Tet-pLKO-puro) vector control or tet-on sh*PD-L1* plasmid and were selected with puromycin. Doxycycline (200 ng/mL, *in vitro*) was added for 48 to 60 hours prior to being verified by immunoblot for PD-L1 expression. Prior to injection, cells were tested to be *Mycoplasma* free. One million cells were resuspended in 30 μL of sterile PBS and injected into both fourth mammary fat pads of 6 to 12 weeks old female SCID/Beiges (10 tumors per group; Charles River). Mice were given fresh doxycycline water (2 mg/mL) every 3 days (starting when average tumor size reached approximately 100 mm^3) until the endpoint. For tumor growth curves, caliper measurements were done every 3 to 4 days, and all the mice of the experimental cohort were necropsied at the same time when the largest tumor within any group reached the endpoint (500–650 mm^3 in volume). For Supplementary Fig. S3, another set of MDA-MB-231 doxycycline-inducible PD-L1 knockdown *in vivo* experiments were performed following the identical procedure described above. Upon tumor establishment, the tumors were extracted after 6 days of doxycycline administration for IHC analysis.

PD-L1 overexpression

MDA-MB-231 cells were infected with pLX317-*PD-L1* plasmid or empty vector control and selected with puromycin. Cells were verified for their PD-L1 expression using PD-L1 XP rabbit antibody (E1L3N). Prior to injection, cells were tested to be *Mycoplasma* free. One million cells were resuspended in 30 μL of sterile PBS and injected into both mammary fat pads of 12-week-old SCID/Beiges (10 tumors per group, Charles River). Caliper measurements were carried out every 3 to 4 days and both groups were necropsied at the same time when the PD-L1–overexpressing tumors reached the endpoint (500–650 mm^3 in volume).

IHC

In vivo mouse xenografts

Breast tumors were fixed in 10% buffered formalin, embedded in paraffin, and sectioned at 4 μm. Antigen retrieval was done in sodium citrate buffer using pressure cooker and incubated overnight at 4°C with antibodies specific for Ki67 (ab15580), cleaved caspase-3 (CST, cat. #9661), and PD-L1 (CST, cat. #13684). All slides were subsequently processed with Vectastain ABC kits (Vector). Slides were scanned using a ScanScope XT Digital Slide Scanner (Aperio) and data were analyzed using Image Scope software.

Patient tumor samples

Studies on resected lung adenocarcinoma patient tumors ($n = 100$) were approved by the ethics boards at the McGill University Health Centre (F11HRR, 17212). Cores with low tumor cellularity and artifacts were not included in the analysis. Cores were stained with the primary antibodies: PD-L1 (CST cat. #13684) 1/100 dilution, and CD44 (ab157107) 1/5,000 dilution. All sections were scanned using an Aperio Scanscope Scanner (Aperio Vista), and images were extracted with Aperio ImageScope.

Flow cytometry

Cells were stained with APC fluorophore-conjugated anti-human PD-L1 (eBioscience, cat. #17-5983-42) at 5 μL of antibody per 200,000 cells and/or PE fluorophore-conjugated anti-human CD44 (BioLegend cat. #103024) at 4.5 μL per 300,000 cells. Unstained cells were used as controls. Aggregates were gated out using FSC-A versus FSC-H and SSC-A versus SSC-H, and live total cells (DAPI-negative) were selected for analysis. Samples were analyzed by BD LSRFortessa Cell Analyzer and FlowJo.

FACS-assisted RNAi genetic screen and data analysis

MDA-MB-231 and BT-549 cells were infected with 11 virus pools (MOI $\sim$ 0.3) and then selected in puromycin for 2 days to obtain successfully transduced cells. Cells with stable shRNA integration were stained with anti–PD-L1–APC (eBioscience) and subjected to fluorescence-activated cell sorting (FACS). The bottom 20% of surface PD-L1 expressing-cells (PD-$L1^{low}$) were collected. Genomic DNA was isolated and shRNA inserts were recovered with PCR amplification performed as described (32). The relative abundance of shRNAs in presort and PD-$L1^{low}$ populations was determined by next-generation sequencing and data were analyzed by MAGeCK statistical software package (33).

Coimmunoprecipitation

BT-549 cells ectopically expressing CD44-ICD alone or together with V5-tagged CREB1 were resuspended in ice-cold lysis buffer [50 mmol/L Tris pH 7.5, 150 mmol/L NaCl, 1% NP40, 1 mmol/L dithiothreitol (DTT), and protease/phosphatase inhibitors) and broken by passing through 20-gauge needles 20 times. After 30-minute incubation on ice, lysates were clarified by centrifugation at 14,000 $\times$ *g* for 15 minutes at 4°C. Supernatant was collected as cell extract, and protein concentrations were determined using Bradford Protein Assay (Bio-Rad). Five micrograms of IgG (abcam ab37415), anti-CREB1 (abcam ab31387), or anti-CD44 (ab157107) antibodies was added to 2 mg of precleared cell lysate in 500 μL of lysis buffer and incubated overnight at 4°C with continuous rocking. Protein immunocomplexes were then incubated with 40 μL protein G sepharose beads (Protein G Sepharose 4 Fast Flow, GE Healthcare) at 4°C for 2 hours. Precipitated proteins were washed 3 times with lysis buffer and eluted with sodium dodecyl sulfate (SDS) loading buffer at 95°C for 10 minutes and analyzed by Western Blot. TrueBlot secondary antibodies (ROCKLAND) were used.

Chromatin immunoprecipitation PCR

The 3–7 $\times$ 10^7 BT-549 and HCC827 cells were fixed in 1% formaldehyde for 10 minutes at room temperature and then quenched with 0.125M glycine for 5 minutes and then incubated on ice for 15 minutes. Fixed cells were pelleted and washed twice with PBS before snap-freezing on dry ice. Cells were lysed successively with three lysis buffers, followed by 10-minute incubation on a rotator at 4°C after each lysis step (Lysis Buffer 1: 50 mmol/L 1 mol/L HEPES-KOH pH

7.5, 140 mmol/L NaCl, 1 mmol/L EDTA, 10% glycerol, 0.5% NP-40, 0.25% Triton X-100; Lysis Buffer 2: 10 mmol/L Tris-HCl pH 8.0, 200 mmol/L NaCl, 1 mmol/L EDTA, 0.5 mmol/L EGTA; Lysis Buffer 3: 10 mmol/L Tris-HCl pH 8.0, 100 mmol/L NaCl, 1 mmol/L EDTA, 0.5 mmol/L EGTA, 0.1% Na-Deoxycholate, 0.5% N-lauroylsarcosine). Cell lysates were sonicated with a Branson 450D Sonifier to sheer DNA into 100-bp to 600-bp fragments. Triton X-100 was added to sonicated lysates and centrifuged at 20,000 × *g* at 4°C to pellet debris. Ten percent of sonicated samples were aliquoted as input. Five micrograms of IgG (abcam ab37415), αCD44 (abcam ab157107, lotGR3247919-7), or αCREB1 (abcam ab31387, lotGR317751-19) antibody was added to the chromatin samples and incubated overnight at 4°C. Protein G Dynabeads (Thermo Fisher Scientific) were added to each IgG and αCD44/αCREB1 sample and incubated for 2 hours at 4°C for antibody pulldown. Immunoprecipitated chromatin was washed with 4 successive buffers (low salt buffer: 20 mmol/L Tris-HCl pH 8.0, 150 mmol/L NaCl, 0.1% SDS, 1% Triton X-100, 2 mmol/L EDTA; medium salt buffer: 20 mmol/L Tris-HCl pH 8.0, 250 mmol/L NaCl, 0.1% SDS, 1% Triton X-100, 2 mmol/L EDTA; LiCl wash: 10 mmol/L Tris-HCl pH 8.0, 250 mmol/L LiCl, 0.5% NP-40, 0.5% Na-deoxycholate, 1 mmol/L EDTA; 1× TE: 10 mmol/L Tris-HCl pH 8.0, 1 mmol/L EDTA). Immunoprecipitated chromatin was then eluted in 150 μL elution buffer (50 mmol/L Tris-HCl pH 8.0, 10 mmol/L EDTA, 1% SDS) and incubated at 65°C for 30 minutes. Elution buffer (100 μL) was added to the Input lysates and incubated together with immunoprecipitated samples overnight at 65°C to denature formaldehyde cross-linking. Samples were digested with RNase A (Thermo Fisher Scientific) and then treated with proteinase K (Sigma-Aldrich) before performing phenol:chloroform extraction. DNA was precipitated with NaCl, glycogen (Fermentas), glycoblue (Ambion), and 100% ethanol overnight at −20°C. Following, DNA was pelleted by 20,000 × *g* for 30 minutes at 4°C, washed with 70% ethanol, and resuspended with 50 μL of 1× TE buffer.

qRT-PCR was performed on immunoprecipitated chromatin using SYBR Green Master Mix (Roche) and the following primers:

CD44-ICD binding site forward, 5′-CCAGCTGCAGCATCTAAGTAA-3′

CD44-ICD binding site reverse, 5′-CCAAGGTCAATGTGTCTAAGAAATG-3′

PD-L1 promoter forward, 5′-GCTTTAATCTTCGAAACTCTTCCC-3′

PD-L1 promoter reverse, 5′-CCTAGGAATAAAGCTGTGTATAGAAATG-3′

GAPDH promoter forward, 5′-CTGAGCAGACCGGTGTCACATC-3′

GAPDH promoter reverse, 5′-GAGGACTTTGGGAACGACTGAG-3′

3.7 kb upstream *PD-L1* forward, 5′-ACCTCACACCTGTGCACTAT-3′

3.7 kb upstream *PD-L1* reverse, 5′-AGCAAGACCTTTCTGCTCTGA-3′

qRT-PCR values from IgG and CD44-ICD were first normalized by the input material. Fold enrichment was calculated as CD44-ICD signal/IgG signal for each sample. For CREB1 chromatin immunoprecipitation (ChIP), qRT-PCR values from IgG and CD44/CREB1 were normalized by the input material.

Chromatin immunoprecipitation tracks

Publicly available ChIP-seq data tracks for H3K27Ac marks were accessed for the following cell lines: MDA-MB-231 (GSE49651; ref. 34), BT-549 (GSE65201; ref. 35), HCC827 (GSE76783; ref. 36), and A549 (37); ChIP-seq track for CREB1 in A549 cells (GSE32465; ref. 38).

Transcriptome data analysis in cancer cell lines and patient tumor samples

The Cancer Cell Line Encyclopedia

The RNA-seq mRNA expression of *PD-L1* and *CD44* in TNBC ($n = 30$) and NSCLC ($n = 143$) cell lines was obtained from the Cancer Cell Line Encyclopedia (CCLE) database (39).

Enriched genes in CD44^{high} patient TNBC and lung adenocarcinoma tumors

RNA-seq mRNA expression of *CD44* (average value of all isoforms) was obtained from TNBC patients (defined as IHC-negative staining for the estrogen receptor and progesterone receptor, and negative or equivocal IHC staining status for HER2) from The Cancer Genome Atlas (TCGA) provisional breast invasive carcinoma cohort ($n = 130$; ref. 40) and TCGA provisional lung adenocarcinoma patient cohort ($n = 250$; ref. 41). The transcriptome of the upper quartile of tumors ranked by *CD44* expression was compared with the lower quartile in both cohorts. Differential expression of genes was analyzed by Bioconductor package DESeq2 (version 1.20.0; ref. 42). The top 48 overlapping genes in TCGA and lung adenocarcinoma (LUAD) cohorts with an adjusted $P < 0.001$ and fold change difference by at least one $\log_2$ are presented.

RNA-seq of patient tumor samples from TCGA PanCancer Atlas

RNA-seq mRNA expression of *CD44* (average value of all isoforms) and *PD-L1* was obtained from 33 cohorts (10,881 patient samples) from the TCGA PanCancer Atlas. 9,010 patients had RNA-seq samples for both *PD-L1* and *CD44*: acute myeloid leukemia ($n = 165$), adrenocortical carcinoma ($n = 76$), bladder urothelial carcinoma ($n = 402$), brain lower grade glioma ($n = 507$), breast invasive carcinoma ($n = 994$), cervical squamous cell carcinoma ($n = 275$), cholangiocarcinoma ($n = 36$), colorectal adenocarcinoma ($n = 524$), diffuse large B-cell lymphoma ($n = 37$), esophageal adenocarcinoma ($n = 181$), glioblastoma multiforme ($n = 145$), head and neck squamous cell carcinoma ($n = 488$), kidney chromophobe ($n = 65$), kidney renal clear cell carcinoma ($n = 352$), kidney renal papillary cell carcinoma ($n = 283$), liver hepatocellular carcinoma ($n = 348$), lung adenocarcinoma ($n = 503$), lung squamous cell carcinoma ($n = 466$), mesothelioma ($n = 82$), ovarian serous cystadenocarcinoma ($n = 201$), pancreatic adenocarcinoma ($n = 168$), pheochromocytoma and paraganglioma ($n = 161$), prostate adenocarcinoma ($n = 168$), sarcoma ($n = 230$), skin cutaneous melanoma ($n = 363$), stomach adenocarcinoma ($n = 407$), testicular germ cell cancer ($n = 141$), thymoma ($n = 119$), thyroid carcinoma ($n = 480$), uterine carcinosarcoma ($n = 56$), uterine corpus endometrial carcinoma ($n = 507$), and uveal melanoma ($n = 80$). TCGA mRNA gene-expression levels were $\log_2$ transformed. Pearson *r* correlations were calculated.

RNA-seq and microarray of patient tumor samples from additional cohorts

RNA-seq analysis was performed on primary tumor samples of 20 different TNBC patients from the Goodman Cancer Research Centre cohort. The average value of all *CD44* isoforms of this RNA-seq data set was used. Affymetrix microarray analysis was performed on samples from 47 TNBC patients from the McGill University cohort, previously characterized by Tofigh and colleagues (GSE58644; ref. 43), and data values are provided as fluorescence intensity. For this data set, the average value of CD44 probes was used (NM_000610;

NM_001001389; NM_001001390; NM_001001391; and NM_001001392). RNA-seq from 42 TNBC primary tumors characterized by Varley and colleagues (GSE58135; ref. 44) was analyzed with the transcripts: *PD-L1* (NM_014143), *CD44* (NM_001001391), and *CREB1* (ENST00000432329.6). Values provided as fragments per kilobase of transcript per million mapped reads (FPKM) with $\log_2$ transformation of *CD44* values. RNA-seq for 87 lung adenocarcinomas characterized by Seo and colleagues (GSE40419; ref. 45) was analyzed with values provided as FPKM with $\log_2$ transformations for the following transcripts: *PD-L1* (NM_014143), *CD44* (NM_001001391), and *CREB1* (NM_004379). RNA-seq of 199 NSCLC patients characterized by Djureinovic and colleagues (GSE81089; ref. 46) was analyzed with values provided as FPKM with $\log_2$ transformations for the transcripts with the following Ensembl gene ID with average value: *PD-L1*: (ENSG00000120217), *CD44*: (ENSG00000026508), and *CREB1* (ENSG00000118260). NanoString data of 22 NSCLC patients characterized by Prat and colleagues (GSE93157; ref. 47) were analyzed with $\log_2$ transformations – value of *CD44* (NM_001001392.1) was used. Pearson *r* correlations were calculated for all cohorts.

Statistical analysis

All statistical analysis of biological replicates was performed using Prism 7 software. Two-tailed Student *t* test, two-way ANOVA, and Pearson correlation statistics were performed as indicated. *, $P < 0.05$; **, $P < 0.01$; ***, $P < 0.001$; ****, $P < 0.0001$. All relevant assays were performed independently at least 3 times.

Results

PD-L1 exerts a cancer cell–intrinsic role in TNBC and NSCLC

TNBC cell lines express higher levels of surface PD-L1 compared with other breast cancer subtypes (22). We hypothesized that PD-L1 may also play a cancer cell–intrinsic role in TNBC as recently shown in other cancer types (12–14). To investigate this, we performed PD-L1 knockdown experiments in MDA-MB-231, BT-549, and HCC1937 TNBC cells, which express the highest PD-L1 protein levels across a panel of breast cancer cells (Supplementary Fig. S1A). Suppression of PD-L1 expression, using two independent shRNAs, strongly inhibited cell proliferation in both short-term cell viability and long-term colony formation assays in these TNBC cells (**Fig. 1A**; Supplementary Fig. S1B). PD-L1 knockdown also resulted in reduced AKT/mTOR signaling, indicated by decreased phosphorylation of AKT and S6 ribosomal protein (rpS6; **Fig. 1B**), which is consistent with previous reports (48). In addition, PD-L1 knockdown led to elevated annexin V and activated caspase-3/7 signals (**Fig. 1C**), indicating apoptosis induction. Conversely, ectopic expression of PD-L1 in TNBC cells increased their cell viability and proliferation with a concomitant increase in AKT activation (Supplementary Fig. S2A–S2C), while also reducing the ability of the mTOR inhibitor Torin to suppress downstream AKT activation (Supplementary Fig. S2D). These results support the tumor-intrinsic role of PD-L1 in TNBC.

To validate *in vivo,* we used orthotopic mouse models by implanting isogenic cell lines of MDA-MB-231 into the mammary fat pads of immunodeficient (SCID-Beige) mice. Using a validated doxycycline-inducible shRNA system (Supplementary Fig. S3A), we allowed mammary tumors to reach 100 mm^3 and then administered doxycycline in the drinking water to induce PD-L1 knockdown (Supplementary Fig. S3B). PD-L1 suppression significantly reduced the growth potential of MDA-MB-231 tumors in this immunodeficient background (**Fig. 1D**), which is consistent with PD-L1 knockdown in 4T1 murine models (31). This decreased growth potential was associated with reduced proliferation in MDA-MB-231 tumors following PD-L1 knockdown (6 days after doxycycline treatment), whereas no significant differences were observed in the apoptotic rate compared with control tumors (Supplementary Fig. S3C and S3D). Conversely, PD-L1 overexpression further enhanced MDA-MB-231 tumor growth *in vivo* (**Fig. 1E**; Supplementary Fig. S4A). Whereas the proliferative rate was comparable between control and PD-L1–overexpressing tumors at the experiment endpoint, we observed a significant decrease in the percentage of apoptotic cells in PD-L1–overexpressing tumors compared with controls (Supplementary Fig. S4B and S4C). Our inability to detect increased proliferation in PD-L1–overexpressing cells likely reflects the fact that the control tumors already possess a high baseline proliferative rate (∼70%; Supplementary Figs. S3C and S4B). Moreover, differences in tumor volumes in the PD-L1 knockdown (∼150 mm^3, early sampling point) versus PD-L1–overexpressing (>500 mm^3, endpoint) tumors likely account for their differential apoptotic rates *in vivo* (Supplementary Figs. S3D and S4C). Combined, these data suggest that tumor intrinsic PD-L1 expression both promotes cell proliferation and reduces apoptosis to increase TNBC growth, irrespective of a T-cell response, which is consistent with our *in vitro* observations (**Fig. 1C**).

In addition to TNBC, NSCLC subtypes harboring activating *RAS* and *EGFR* mutations have been shown to express high levels of PD-L1 (15–18). We therefore investigated the potential cancer cell–intrinsic role of PD-L1 in NSCLC. We detected strong total PD-L1 protein expression in many NSCLC cell lines: *RAS*-mutant H358, A549, and H1915; *EGFR*-mutant HCC827; *ROS1*-translocated HCC78; *MET*-amplified EBC-1 (Supplementary Fig. S5A). Similar to TNBC, knockdown of PD-L1 strongly reduced the clonogenic potential of NSCLC cells (HCC827, H358, A549, and H1915) concomitant with suppressed AKT and rpS6 phosphorylation (**Fig. 1F** and **G**; Supplementary Fig. S5B and S5C) and increased apoptosis as indicated by elevated staining of annexin V and activated caspase-3/7 (**Fig. 1H**). Together, our findings established a tumor-intrinsic role of PD-L1 in increasing the tumorigenic potential of TNBC and NSCLC through promoting cell survival.

FACS-assisted shRNA screen identifies CD44 as a novel positive regulator of PD-L1

Given the immunosuppressive and tumor-intrinsic roles of PD-L1, it is important to delineate the underlying mechanisms controlling tumor PD-L1 expression. Previous studies have implicated the AKT and ERK signaling pathways in the regulation of PD-L1 expression in breast cancer, NSCLC, and melanoma (2, 20–22). We explored their ability to suppress PD-L1 expression by treating 5 TNBC cell lines with the AKT inhibitor MK-2206 or MEK inhibitor trametinib, alone or in combination. Although these treatments resulted in partial or complete growth inhibition of these cells, they failed to consistently and appreciably suppress PD-L1 expression (Supplementary Fig. S6A and S6B). These results highlight the need to uncover other regulators of PD-L1 expression that can be exploited therapeutically.

To address this issue in an unbiased manner, we compiled a focused shRNA library against ∼1,200 known target genes of clinically approved drugs (both antagonists and agonists). An RNAi-based approach was chosen to better mimic pharmacologic modulation. MDA-MB-231 and BT-549 cells, which express high surface PD-L1 levels (Supplementary Fig. S7A and S7B), were infected with the shRNA library and quickly selected for stable integration followed by isolation of the cell population with low surface expression levels of PD-L1 (PD-$L1^{low}$; bottom 20%) using FACS (**Fig. 2A**). Upon screen completion, we analyzed the data using the MAGeCK statistical

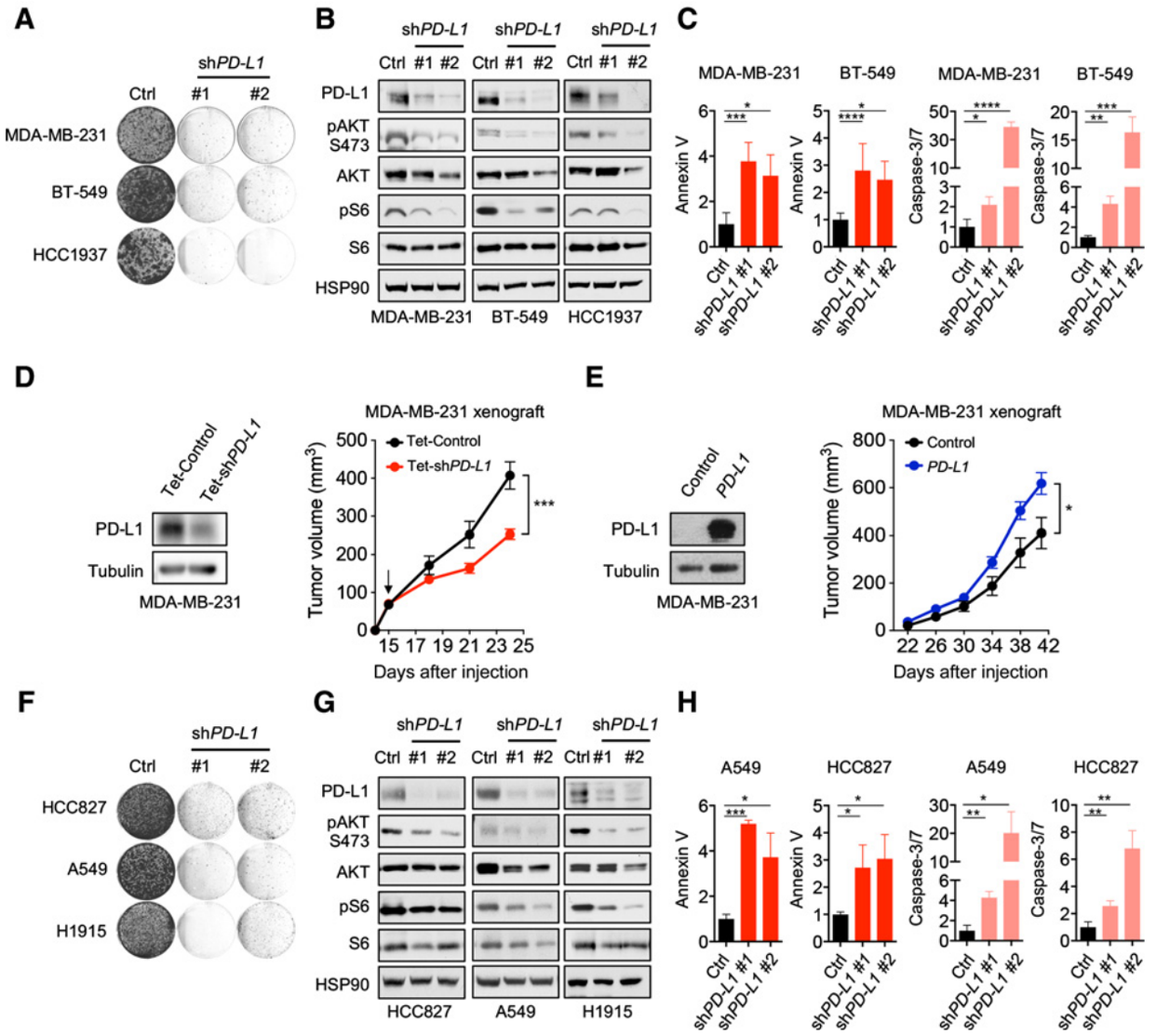

Figure 1.

Tumor-intrinsic function of PD-L1 in TNBC and NSCLC. **A,** Long-term colony formation proliferation assays of TNBC cell lines after PD-L1 knockdown. Cells were grown for 8–10 days. **B,** Immunoblot analysis of AKT/mTOR signaling pathways after PD-L1 knockdown in TNBC cell lines. **C,** Annexin V and activated caspase-3/7 staining after PD-L1 knockdown in MDA-MB-231 and BT-549 cell lines. Fluorescence measured with IncuCyte Zoom Live-Cell Analysis System. *, $P < 0.05$; **, $P < 0.01$; ***, $P < 0.001$; ****, $P < 0.0001$; Student *t* test. **D,** Orthotopic *in vivo* xenograft experiments of MDA-MB-231 tumors expressing a control vector or doxycycline-inducible sh*PD-L1* #2 (Tet-*shPD-L1)*. Immunoblot validation of PD-L1 knockdown preimplantation is shown on the left. Tumors ($n = 5$ mice per group, 10 tumors per group) were implanted in the mammary glands of SCID mice, and doxycycline was given daily starting on day 15 (arrow). Mean tumor volumes are shown ±SEM. ***, $P < 0.001$; two-way ANOVA. **E,** Orthotopic *in vivo* xenograft experiments of MDA-MB-231 tumors ectopically expressing a control vector or *PD-L1* cDNA. Immunoblot validation of ectopic PD-L1 expression preimplantation is shown on the left. Tumors ($n = 5$ mice per group, 10 tumors per group) were implanted in the mammary glands of SCID mice. Mean tumor volumes are shown ±SEM. *, $P < 0.05$; two-way ANOVA. **F,** Long-term colony formation proliferation assays of NSCLC cell lines after PD-L1 knockdown. Cells were grown for 8–14 days. **G,** Immunoblot analysis of AKT/mTOR signaling pathways after PD-L1 knockdown in NSCLC cell lines. **H,** Annexin V and activated caspase-3/7 staining after PD-L1 knockdown in A549 and HCC827 NSCLC cell lines. *, $P < 0.05$; **, $P < 0.01$; ***, $P < 0.001$; Student *t* test. Fluorescence measured with IncuCyte Zoom Live-Cell Analysis System.

software package (33) to identify genes whose suppression was enriched in the PD-L1^{low} population compared with the parental population immediately prior to FACS sorting. As shown in **Fig. 2B** and Supplementary Table S1, *PD-L1* was identified as the top-ranked gene from both cell lines, which validates the screens. In addition, *CD44*, a well-established cancer stem cell marker and membrane receptor necessary for an epithelial-to-mesenchymal transition (EMT; refs. 49, 50), was the next top-ranked candidate that was shared between both cell lines (**Fig. 2B**; Supplementary Table S1). These unbiased analyses indicate that *CD44* may be a critical positive regulator of PD-L1 expression in TNBC.

Validating the role of CD44 in regulating PD-L1 expression, knockdown of CD44 using two independent shRNAs resulted in strong suppression of both PD-L1 protein expression and growth in

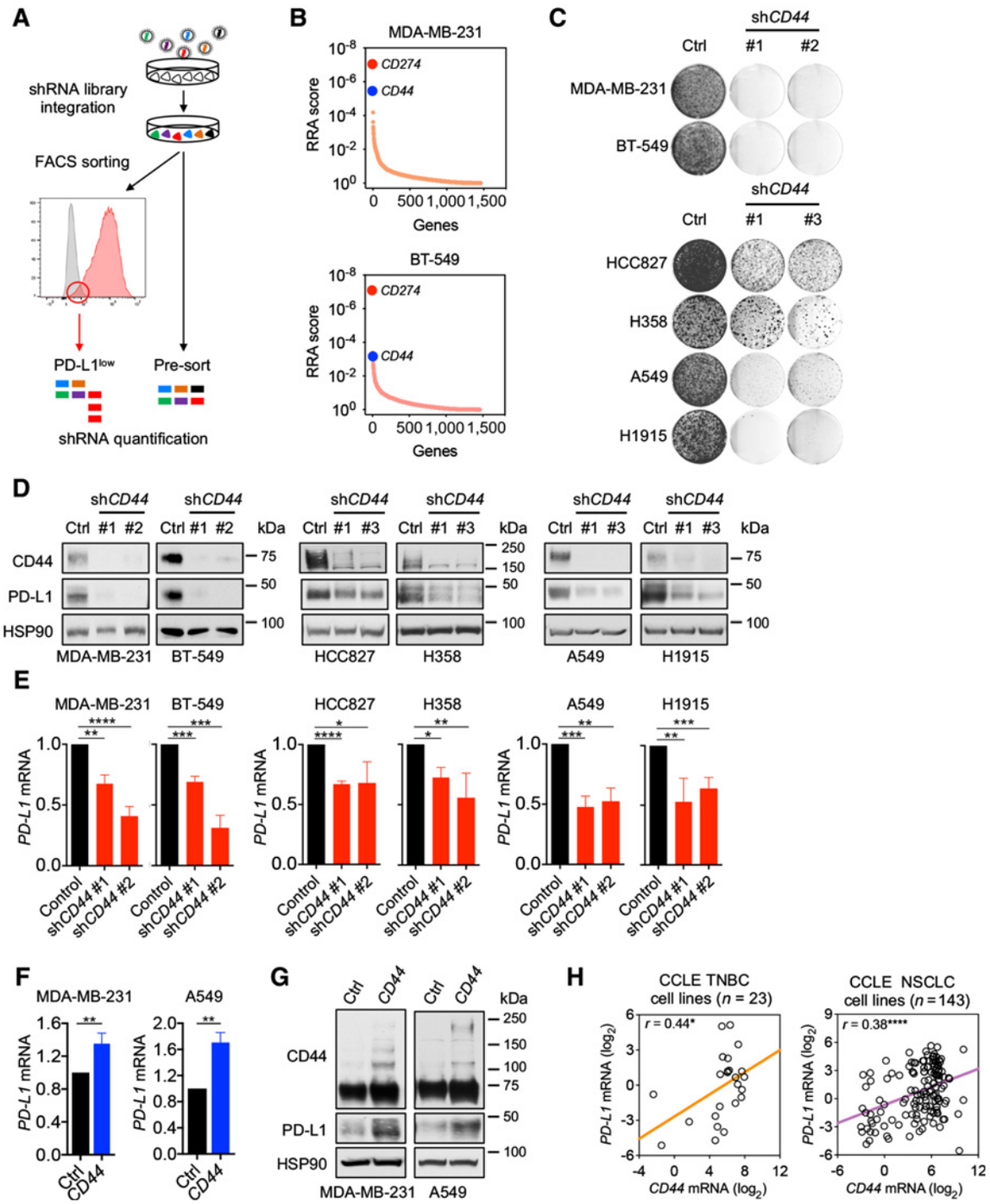

Figure 2.

CD44 is a novel positive regulator of PD-L1 in TNBC and NSCLC **A,** Schematic of FACS-assisted shRNA screen to identify positive regulators of PD-L1 expression in TNBC. **B,** FACS-assisted shRNA screen identifies *CD44* as a novel, positive regulator in MDA-MB-231 and BT-549. MAGeCK computational analysis ranks *PD-L1* as the top hit in both cell lines. *CD44* is the next top candidate shared between both cell lines. Hits were ranked according to robust rank aggregation (RRA) score. **C,** Long-term colony formation proliferation assays of TNBC (top) and NSCLC (bottom) cell lines after CD44 knockdown. Cells were grown for 8–14 days. **D,** Immunoblot analysis of PD-L1 expression after CD44 knockdown in TNBC and NSCLC cell lines. **E,** qRT-PCR analysis of *PD-L1* expression after CD44 knockdown in TNBC and NSCLC cell lines. **F,** qRT-PCR analysis of *PD-L1* mRNA after ectopic CD44 expression in TNBC and NSCLC cell lines. **G,** Immunoblot analysis of PD-L1 expression after ectopic expression of CD44 (NM_001001389.1; 76 kDa when unmodified) in TNBC and NSCLC cell lines. **H,** Pearson correlation of *PD-L1* and *CD44* mRNA in TNBC ($n = 23$) and NSCLC ($n = 143$) cell lines from the CCLE RNA-seq database. *, $P < 0.05$; **, $P < 0.01$; ***, $P < 0.001$; ****, $P < 0.0001$; Student t test.

both MDA-MB-231 and BT-549 cell lines (**Fig. 2C** and **D**). In addition, CD44 suppression resulted in a significant decrease of *PD-L1* mRNA expression in these cells (**Fig. 2E**), albeit to a lesser extent than the observed reduction in PD-L1 protein levels. These data suggest that CD44 may regulate PD-L1 at both the transcriptional and posttranscriptional levels. Ectopic expression of PD-L1 did not rescue the growth inhibition of CD44 knockdown (Supplementary Fig. S8A and S8B), indicating that CD44 also promotes cancer cell growth through PD-L1–independent pathways. This is expected as CD44 participates in a wide variety of critical cellular processes (49, 50).

Consistent with a role for CD44 in regulating PD-L1 expression, we observed a positive correlation between CD44 and PD-L1 expression levels in our TNBC and NSCLC cell line panels (Supplementary Fig. S9A–S9D). Supporting this, FACS analysis in 6 representative cell lines (MDA-MB-231, BT549, H358, H1915, A549, and HCC827) showed a significant and linear positive correlation between CD44 and PD-L1 surface expression among individual subpopulations of cells within each cell line (R Pearson = 0.88–0.99; Supplementary Fig. S10A and S10B).

Given the above observations in NSCLC cells, we investigated the potential genetic interaction between CD44 and PD-L1 in this context. Indeed, CD44 knockdown also suppressed PD-L1 expression and the long-term clonogenic potential of NSCLC cells (**Fig. 2C–E**). Complementary to the knockdown results, ectopic CD44 expression in TNBC and NSCLC cells led to increased PD-L1 mRNA (**Fig. 2F**) and protein (**Fig. 2G**) expression. Independently supporting our data, we observed significant positive correlations between *CD44* and *PD-L1* mRNA expression in 23 TNBC ($r = 0.44$, $P = 0.0311$) and 143 NSCLC cell lines ($r = 0.38$, $P < 0.0001$) from the CCLE database (**Fig. 2H**; ref. 39). Taken together, these results demonstrate that CD44 plays a key role in positively regulating PD-L1 expression in both TNBC and NSCLC cells.

CD44 activates *PD-L1* transcription partly through its cleaved intracellular domain

Our above data indicate that CD44 promotes PD-L1 expression in part through transcriptional regulation. CD44 is known to be cleaved by metalloproteases extracellularly, leaving behind a membrane-bound C-terminal fragment that subsequently undergoes intramembranous cleavage by gamma-secretase to release an intracellular domain (CD44-ICD; ref. 51). CD44-ICD, which is shared by all dominant CD44 isoforms (52), can then translocate into the nucleus where it acts as a transcription factor through binding to its consensus DNA sequence and promote tumorigenesis (53, 54). Therefore, we investigated the potential role of the CD44-ICD in regulating *PD-L1* expression.

We first confirmed the expression of CD44-ICD in TNBC (MDA-MB-231, BT-549) and NSCLC (HCC827, A549) cells by CD44 knockdown, which suppressed generation of CD44-ICD concomitant with reduced PD-L1 expression (**Fig. 3A**). Conversely, ectopic CD44 expression increased CD44-ICD in TNBC and NSCLC cells (Supplementary Fig. S11). Ectopic expression of CD44-ICD alone in TNBC and NSCLC cell lines was sufficient to increase PD-L1 mRNA and protein levels (**Fig. 3B** and **C**). Endogenous expression of full-length CD44 was also elevated upon CD44-ICD overexpression (**Fig. 3B**), because CD44 itself is a transcriptional target of CD44-ICD through a positive-feedback loop (51). Elevated CD44-ICD expression also increased the growth potential of TNBC and NSCLC cell lines (Supplementary Fig. S12), consistent with our PD-L1 overexpression results (Supplementary Fig. S2B and S2C). Furthermore, ectopic CD44-ICD expression partially restored PD-L1 levels in BT-549 and HCC827 cells expressing an shRNA that specifically targets endogenous full-length CD44 but not the exogenous CD44-ICD (**Fig. 3D**). We also examined if perturbation of endogenous CD44-ICD cleavage can alter PD-L1 expression. Hyaluronic acid (HA) is the cognate ligand for CD44 and stimulates cell migration, proliferation, and CD44 cleavage (55). Treatment of MDA-MB-231 cells with low-molecular-weight HA increased proliferation and CD44-ICD generation, as well as elevated PD-L1 mRNA and protein expression (**Fig. 3E–G**). This HA-induced proliferation was suppressed upon PD-L1 knockdown (Supplementary Fig. S13), suggesting this growth promoting function of CD44 may require PD-L1. Together, these complementary data support the notion that CD44 activates *PD-L1* expression, in part, through its ICD fragment.

Given the known role of CD44-ICD as a transcription factor, we next investigated if the CD44-ICD can directly regulate *PD-L1* expression. Using ChIP, we detected CD44-ICD occupancy in the promoter region of *PD-L1* (*PD-L1*p) but not in the control *GAPDH* promoter region (*GAPDH*p), in both BT-549 and HCC827 cells ectopically expressing CD44-ICD (**Fig. 3H**). Although this *PD-L1* promoter region does not contain a CD44-ICD consensus binding sequence "CCTGCG" (54), it contains a binding site for the CREB1 transcription factor (Supplementary Fig. S14; ref. 38), which is known to bind CD44-ICD to activate transcription of other oncogenes (56). This suggests that CD44-ICD could be recruited to this *PD-L1* promoter region through CREB1. Furthermore, we also detected CD44-ICD occupancy at a CD44-ICD consensus binding sequence "CCTGCG" in the first intron of the *PD-L1* locus (**Fig. 3H**), which contains other known regulatory elements (57) and is enriched for active regulatory marks such as H3K27Ac (Supplementary Fig. S14; refs. 34–37). We also observed this selective enrichment in these cells expressing control vector but to a lesser extent likely due to the lower basal CD44-ICD expression (**Fig. 3H**). Together, these results are consistent with a model that CD44-ICD can directly regulate *PD-L1* transcription.

Our above observation of the *PD-L1* promoter region containing a CREB1 binding site prompted us to investigate the potential involvement of CREB1 in mediating *PD-L1* regulation. Knockdown of CREB1 in BT-549, MDA-MB-231, A549, and HCC827 cells suppressed PD-L1 expression (**Fig. 3I** and **J**; Supplementary Fig. S15), indicating that CREB1 is an activator of PD-L1 expression. A direct interaction between CREB1 and CD44-ICD in regulating *CCND1* expression has been documented in thyroid cancer cells (56). Consistent with this, we found that CD44-ICD and CREB1 coimmunoprecipitate in BT-549 cells ectopically expressing CD44-ICD alone or together with CREB1 (Supplementary Fig. S16A and S16B). Using ChIP, we found robust CREB1 occupancies at both regions of the *PD-L1* locus where CD44-ICD binding was also detected in BT-549 cells (**Fig. 3K**). Moreover, these CREB1 occupancies were both elevated when CD44-ICD was overexpressed and reduced when CREB1 was knocked down. Together, these data suggest that CREB1 may cooperate with CD44-ICD to regulate *PD-L1* transcription but do not rule out the possibility where they also act independently to control *PD-L1* expression.

CD44 positively correlates with PD-L1 expression in patient tumors

To further validate our above findings, we analyzed the expression of CD44 and PD-L1 in multiple patient tumor collections. We first investigated the RNA-seq data of TNBC ($n = 130$; ref. 40) and LUAD ($n = 250$; ref. 41), a main NSCLC subtype, from TCGA. We compared the transcriptomes of the top quartile of *CD44*-expressing patient tumors ($CD44^{high}$) against the bottom quartile and found that *PD-L1* was among the overlapping genes whose expression was significantly

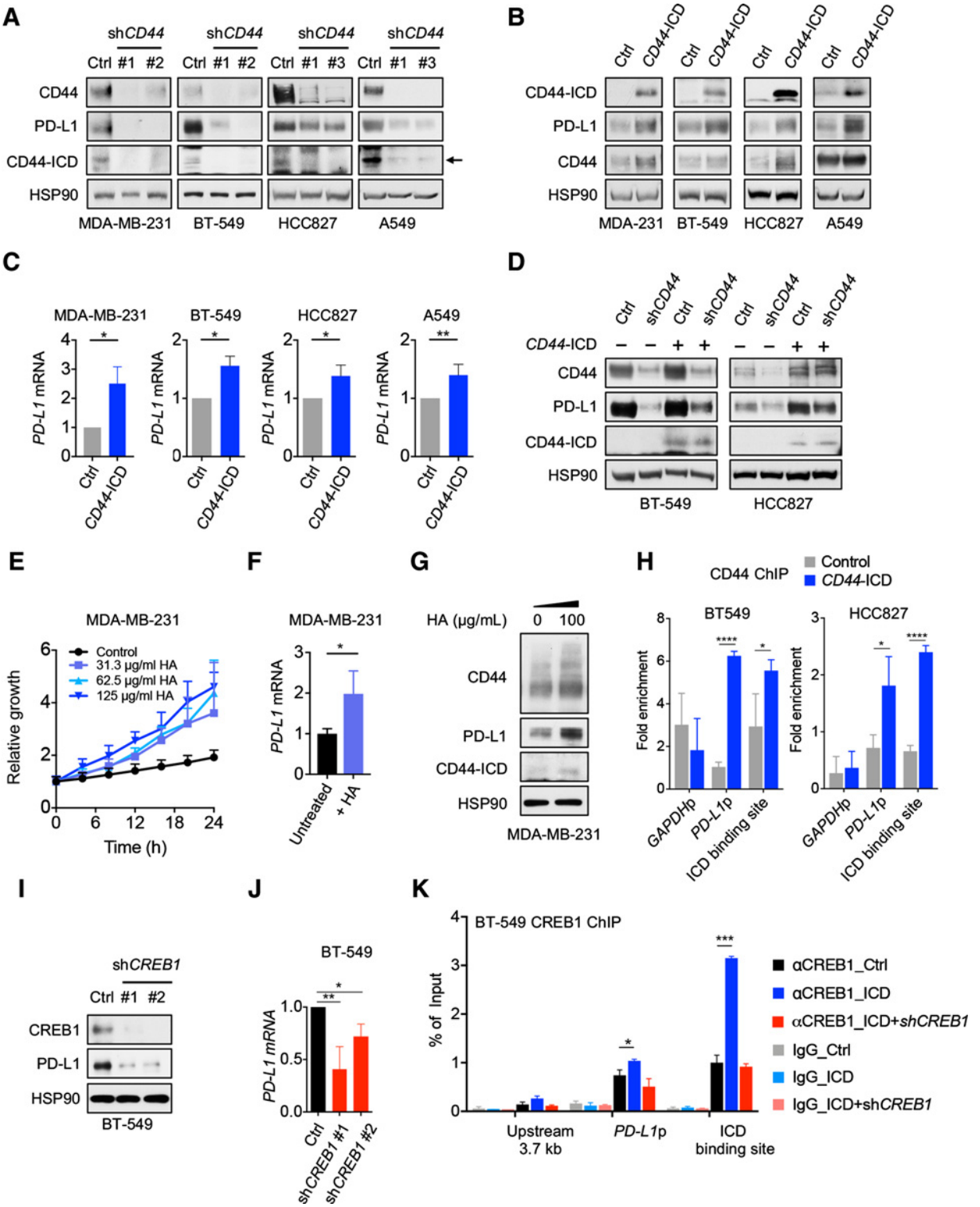

Figure 3.

The CD44 intracellular domain promotes *PD-L1* transcription in TNBC and NSCLC. **A,** Immunoblot analysis showing reduced PD-L1 expression after CD44 knockdown is concomitant with suppressed formation of CD44-ICD in TNBC and NSCLC cell lines. ICD, intracellular domain. **B,** Immunoblot analysis of PD-L1 and CD44 expression after ectopic expression of CD44-ICD in TNBC and NSCLC cell lines. **C,** qRT-PCR analysis of *PD-L1* mRNA after ectopic expression of CD44-ICD in TNBC and NSCLC cell lines. (*Continued on the following page.*)

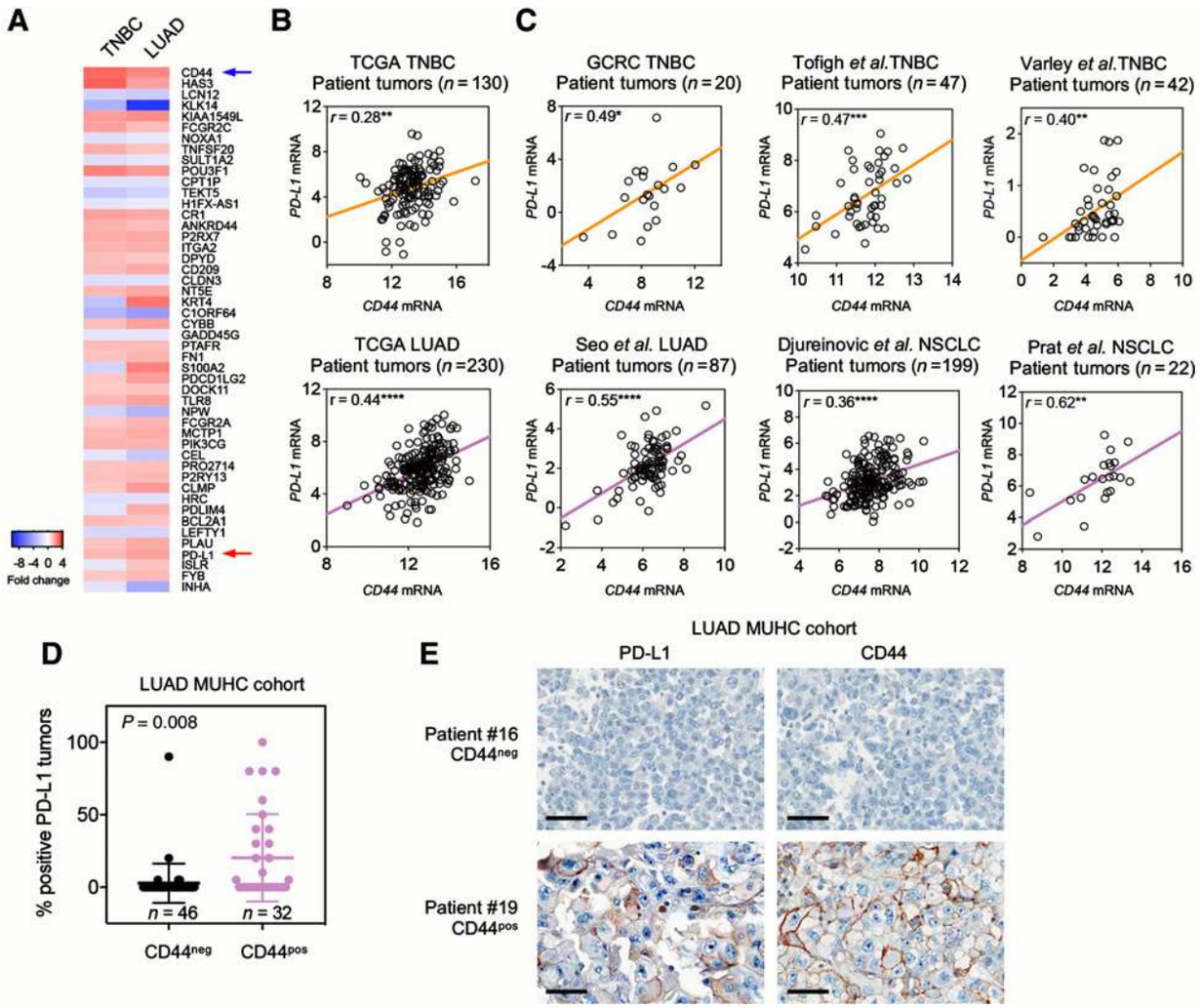

Figure 4.

Correlation of CD44 and PD-L1 expression in TNBC and NSCLC patient tumors **A,** Heat map of the top 48 shared genes showing differential RNA-seq gene expression in *CD44*^{high} TNBC and LUAD TCGA patient tumors compared with *CD44*^{low} patient tumors. Both *CD44* and *PD-L1* are among the top, overlapping enriched genes in the *CD44*^{high} population. **B,** Pearson correlation of *PD-L1* and *CD44* RNA-seq mRNA expression in TNBC and LUAD TGCA patient tumors. **C,** Pearson correlation of *PD-L1* and *CD44* RNA-seq mRNA expression in patient tumors from additional TNBC, LUAD, and NSCLC cohorts. **D,** CD44-positive patient tumors express higher PD-L1 protein compared with CD44-negative patient tumors. IHC was utilized to score PD-L1 and CD44 protein expression in the LUAD MUHC Cohort tissue microarray. **E,** Representative IHC staining of PD-L1 and CD44 protein in LUAD patient tumors. CD44 and PD-L1 IHC staining are negative for patient #16. Patient #19 has positive CD44 (60%) and PD-L1 (40%) IHC staining. Scale bar, 50 μm. *, $P < 0.05$; **, $P < 0.01$; ***, $P < 0.001$; ****, $P < 0.0001$; Student *t* test.

(*Continued.*) **D,** Immunoblot showing ectopic exogenous CD44-ICD expression partially rescues PD-L1 expression after knockdown of endogenous CD44 in TNBC and NSCLC cell lines. **E,** Short-term proliferation assay of MDA-MB-231 cells treated with elevating concentrations of low-molecular-weight HA over 24 hours. **F,** qRT-PCR analysis of *PD-L1* after treatment with 100 μg/mL of low-molecular-weight HA for 24 hours. **G,** Immunoblot analysis of PD-L1 after treatment with 100 μg/mL of low-molecular-weight HA for 24 hours. **H,** qRT-PCR following chromatin immunoprecipitation showing elevated binding at both the CD44-ICD consensus binding site and *PD-L1* promoter locus (*PD-L1*p) in TNBC and NSCLC cells ectopically expressing CD44-ICD compared with a control vector. IgG or anti-CD44-ICD antibodies were utilized in the pulldown. qRT-PCR values from IgG and CD44-ICD were first normalized by the input material. Fold enrichment was calculated as CD44-ICD signal/IgG signal for each sample. The *GAPDH* promoter locus (*GAPDH*p) was utilized as a negative control. **I,** Immunoblot analysis showing reduced PD-L1 expression after CREB1 knockdown in BT-549. **J,** qRT-PCR analysis of *PD-L1* expression after CREB1 knockdown in BT-549. **K,** qRT-PCR following chromatin immunoprecipitation at the CD44-ICD consensus binding site and at the PD-L1 promoter regions in BT-549 cells. Cells were ectopically expressing a control vector (Ctrl), CD44-ICD (ICD), or CD44-ICD plus a shRNA against *CREB1* (ICD + sh*CREB1*). IgG or anti-CREB1 antibodies were utilized in the pulldown. qRT-PCR values from IgG and CREB1 were normalized by the input material. The 3.7 kb upstream of the transcription start site of the *PD-L1* locus was utilized as a control. *, $P < 0.05$; **, $P < 0.01$; *** $P < 0.001$; ****, $P < 0.0001$; Student *t* test.

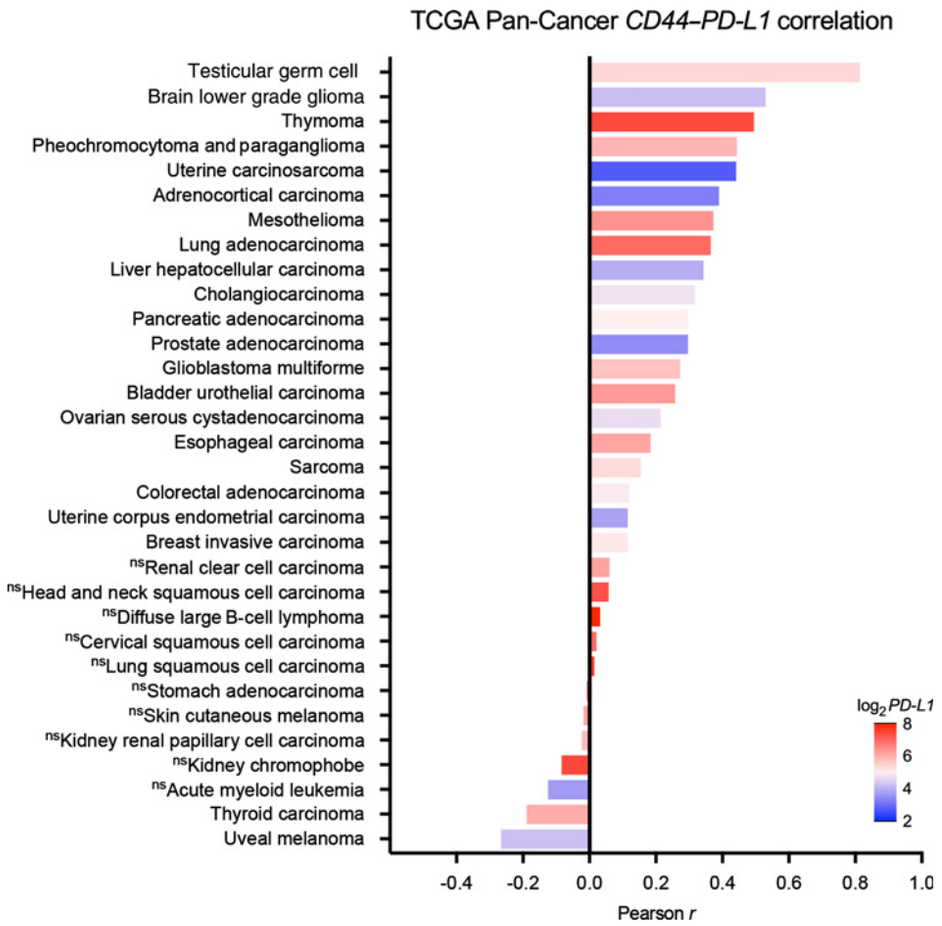

Figure 5.
Pan-cancer correlation of *PD-L1* and *CD44* expression in patient tumors. Pearson correlation of *PD-L1* and *CD44* RNA-seq mRNA gene expression across 33 different tumor types from TCGA. Color intensity of histograms representative of mean $\log_2$ *PD-L1* expression across each tumor cohort.

elevated in $CD44^{high}$ tumors (**Fig. 4A**). Furthermore, we observed a significant correlation between *CD44* and *PD-L1* mRNA expression in these cohorts of TNBC ($r = 0.28$, $P = 0.0011$) and NSCLC ($r = 0.44$, $P < 0.0001$; **Fig. 4B**). Similar correlation was also observed in an independent cohort of primary TNBC tumors ($r = 0.49$, $P = 0.0276$) as well as in five additional publicly available patient tumor collections of TNBC ($r = 0.47$, $P = 0.0008$; $r = 0.40$, $P = 0.0079$; refs. 43, 44), LUAD ($r = 0.55$, $P < 0.0001$; ref. 45), and NSCLC ($r = 0.36$, $P < 0.0001$; $r = 0.62$, $P = 0.0021$; **Fig. 4C**; refs. 46, 47). Consistent with our cell line data, we also observed a positive correlation of *CREB1* and *PD-L1* mRNA levels in the majority of these data sets, although only 4 are significant: including both TGCA cohorts: TNBC ($r = 0.30$, $P = 0.0005$; ref. 40) and LUAD ($r = 0.16$, $P = 0.0129$; ref. 41) cohorts along with another TNBC cohort ($r = 0.45$, $P = 0.0026$; ref. 44) and NSCLC cohort ($r = 0.54$, $P = 0.0095$; Supplementary Fig. S17A and S17B; ref. 47).

Using IHC, we also analyzed protein expression of CD44 and PD-L1 in an additional patient primary tumor collection of NSCLCs ($n = 78$). We found that CD44 IHC-positive ($CD44^{pos}$) NSCLC tumors expressed significantly higher levels of PD-L1 protein compared with CD44 IHC-negative ($CD44^{neg}$) tumors ($P = 0.008$; **Fig. 4D** and **E**). Collectively, these results support our *in vitro* data and establish that CD44 is a critical positive regulator of PD-L1 in TNBC and NSCLC.

Lastly, to extend our findings beyond TNBC and NSCLC, we investigated the potential correlation between *CD44* and *PD-L1* mRNA expression in over 9,000 TCGA patient tumors across 33 different cancer types (58). As shown in **Fig. 5**, Pearson correlation analysis demonstrates a positive and significant correlation between *CD44* and *PD-L1* in the cohorts encompassing the majority of distinct cancers. These findings suggest that the connection between CD44 and PD-L1 may also be a general genetic interaction preserved among diverse cancer types, and highlight CD44 as a novel potential therapeutic target to suppress PD-L1 tumor–intrinsic function.

Discussion

Our study establishes the cancer cell–intrinsic role of PD-L1 in TNBC and NSCLC and uncovers that CD44 is a critical positive regulator of PD-L1 expression in these cancers. We demonstrate that CD44 activates *PD-L1* expression in part through its cleaved cytoplasmic domain CD44-ICD.

We provide *in vitro* and *in vivo* data establishing the critical role of PD-L1 in promoting proliferation and survival of TNBC and NSCLC cells associated with AKT/mTOR signaling, independent of its immunosuppressive activity. This is consistent with previous reports in other cancer types such as sarcomas, ovarian cancer, and melanoma (13, 14). Using an unbiased functional genetics approach, we then identify CD44 as a critical and novel regulator of PD-L1 expression in TNBC and NSCLC. Our findings suggest that the tumorigenicity of CD44, a canonical cancer stem cell marker, is partly through promoting PD-L1 expression that mediates cancer cell proliferation and immune evasion. In line with this, basal cancer stem cells have been associated with

immune suppression and HA activation of CD44 was shown to increase tumor-associated macrophage infiltration, which themselves contribute to dampening the immune response (59, 60). In addition, PD-L1 expression has been linked to resistance to chemotherapy in breast and prostate cancer cells (12), which may mediate chemoresistance of cancer stem cells.

Mechanistically, we demonstrate that CD44 regulates *PD-L1* expression through its ICD. We establish this regulation in TNBC and NSCLC cells by ectopically expressing CD44-ICD and manipulating the cleavage of endogenous CD44-ICD with HA. Consistent with the established role of CD44-ICD as a transcription factor (53, 54), we detected its occupancy at a CD44-ICD consensus–binding site located in the regulatory region of the *PD-L1* locus within the first intron in TNBC and NSCLC cells. We also detected CD44-ICD binding at the promoter region of *PD-L1*. Although this region lacks the consensus CD44-ICD–binding sequence, a CREB1-binding site is present. Because CD44-ICD can interact with CREB-binding protein (CBP)/p300 to activate *CCND1* transcription (51, 56), similar regulation may also be in place for *PD-L1*. Supporting this, our ChIP data in BT-549 cells showed CREB1 occupancy at this CREB1-binding site region of the *PD-L1* promoter as well as the CD44-ICD consensus–binding site region. Furthermore, suppression of CREB1 also reduced PD-L1 in these cells. However, whether CREB1 and CD44-ICD cooperate or independently regulate PD-L1 expression remains to be further studied.

Transcriptional regulation of *PD-L1* by CD44 is further supported by multiple expression data sets of cell lines and patient tumor samples analyzed. However, we only found significant positive correlations between *CREB1* and *PD-L1* in half of the same tumor expression data sets analyzed, suggesting that CD44 plays a dominant role in regulating *PD-L1* expression. Supporting our findings, the positive correlation between CD44 and PD-L1 expression has also been reported by others in TNBC and NSCLC as well as head and neck cancer (61–63). This CD44/PD-L1 genetic interaction may also be preserved in other cancer types as suggested by our pan-cancer expression data analysis.

In addition to transcriptional regulation, CD44 likely also regulates PD-L1 posttranscriptionally. We observed a substantial effect of CD44 on PD-L1 protein expression compared with transcriptional regulation, suggesting that posttranscriptional mechanisms may play a dominant role in controlling PD-L1 levels. This remains to be investigated. Although CD44-ICD is shared by all dominant CD44 isoforms (52), our data do not rule out additional mechanisms that may be isoform-specific. It has been also reported that PD-L1 knockdown in MDA-MB-231 cells showed signs of EMT reversal, including partial suppression of CD44 surface expression (64), further highlighting the complexity of the genetic interaction between CD44 and PD-L1. Although our initial intention was to identify druggable regulators of PD-L1, CD44 remains hard to target therapeutically as initial clinical trials attempting to block the CD44–HA interaction yielded only marginal responses (65). In principle, gamma-secretase inhibitors could be used to inhibit endogenous CD44-ICD cleavage to suppress PD-L1 expression. However, gamma secretases cleave additional targets, other than CD44, and their inhibition may lead to unwanted effects. Thus, alternative druggable regulators of PD-L1 are yet to be uncovered.

In summary, our study uncovers that CD44 is a critical regulator of PD-L1 expression in TNBC and NSCLC, where PD-L1 exerts a tumor-intrinsic role. Our findings provide novel mechanistic sights for the well-established role of CD44 as a cancer stem cell marker—high PD-L1 expression of CD44 populations may in part contribute to their tumorigenic, immunosuppressive, and chemoresistant traits. Thus, the CD44/PD-L1 axis is a critical therapeutic target for cancer treatment.

Disclosure of Potential Conflicts of Interest

No potential conflicts of interest were disclosed.

Authors' Contributions

Conception and design: T. Kong, J. Ursini-Siegel, S. Huang
Development of methodology: T. Kong, R. Ahn, X. Zhu, Y. Xue, M.-C. Guiot, S. Huang
Acquisition of data (provided animals, acquired and managed patients, provided facilities, etc.): T. Kong, R. Ahn, K. Yang, X. Zhu, G. Morin, R. Bramley, N.C. Cliffe, Y. Xue, Q. Li, S. Jung, A.V. Gonzalez, S. Camilleri-Broet, M.-C. Guiot, M. Park
Analysis and interpretation of data (e.g., statistical analysis, biostatistics, computational analysis): T. Kong, R. Ahn, K. Yang, X. Zhu, Z. Fu, G. Morin, N.C. Cliffe, Y. Xue, H. Kuasne, Q. Li, M.-C. Guiot, J. Ursini-Siegel
Writing, review, and/or revision of the manuscript: T. Kong, R. Ahn, K. Yang, Z. Fu, N.C. Cliffe, Y. Xue, A.V. Gonzalez, M. Park, J. Ursini-Siegel, S. Huang
Administrative, technical, or material support (i.e., reporting or organizing data, constructing databases): T. Kong, H. Kuasne, A.V. Gonzalez, M. Park
Study supervision: T. Kong, M. Park, J. Ursini-Siegel, S. Huang

Acknowledgments

We thank Giulio Aceto, Bianca Adams, and Laure Poittevin De La Frégonnière for support. S. Huang is supported by Canadian Institutes of Health Research (CIHR) grants MOP-130540 and PJT-156233. J. Ursini-Siegel and S. Huang acknowledge funding from the Canadian Cancer Society Research Institute (CCSRI) grant #705189 and Cancer Research Society (CRS) grant #23575. T. Kong is supported by Canderel. R. Ahn is supported by the MICRTP doctoral award.

The costs of publication of this article were defrayed in part by the payment of page charges. This article must therefore be hereby marked *advertisement* in accordance with 18 U.S.C. Section 1734 solely to indicate this fact.

Received April 8, 2019; revised September 18, 2019; accepted November 8, 2019; published first November 13, 2019.

References

1. Freeman GJ, Long AJ, Iwai Y, Bourque K, Chernova T, Nishimura H, et al. Engagement of the PD-1 immunoinhibitory receptor by a novel B7 family member leads to negative regulation of lymphocyte activation. J Exp Med 2000;192:1027–34.
2. Chen N, Fang W, Zhan J, Hong S, Tang Y, Kang S, et al. Upregulation of PD-L1 by EGFR activation mediates the immune escape in EGFR-Driven NSCLC: implication for optional immune targeted therapy for NSCLC patients with EGFR mutation. J Thorac Oncol 2015;10:910–23.
3. Smyth MJ, Ngiow SF, Ribas A, Teng MW. Combination cancer immunotherapies tailored to the tumour microenvironment. Nat Rev Clin Oncol 2016;13:143–58.
4. Bianchini G, Balko JM, Mayer IA, Sanders ME, Gianni L. Triple-negative breast cancer: challenges and opportunities of a heterogeneous disease. Nat Rev 2016; 13:674–90.
5. Carey LA, Dees EC, Sawyer L, Gatti L, Moore DT, Collichio F, et al. The triple negative paradox: primary tumor chemosensitivity of breast cancer subtypes. Clin Cancer Res 2007;13:2329–34.
6. Schmid P, Adams S, Rugo HS, Schneeweiss A, Barrios CH, Iwata H, et al. Atezolizumab and nab-paclitaxel in advanced triple-negative breast cancer. N Engl J Med 2018;379:2108–21.
7. Nanda R, Chow LQ, Dees EC, Berger R, Gupta S, Geva R, et al. Pembrolizumab in patients with advanced triple-negative breast cancer: phase Ib KEYNOTE-012 study. J Clin Oncol 2016;34:2460–7.
8. Miyoshi H, Kiyasu J, Kato T, Yoshida N, Shimono J, Yokoyama S, et al. PD-L1 expression on neoplastic or stromal cells is respectively a poor or good prognostic factor for adult T-cell leukemia/lymphoma. Blood 2016;128: 1374–81.

9. Wu SP, Liao RQ, Tu HY, Wang WJ, Dong ZY, Huang SM, et al. Stromal PD-L1-positive regulatory T cells and PD-1-positive CD8-positive T cells define the response of different subsets of non-small cell lung cancer to PD-1/PD-L1 blockade immunotherapy. J Thorac Oncol 2018;13:521–32.
10. Li X, Wetherilt CS, Krishnamurti U, Yang J, Ma Y, Styblo TM, et al. Stromal PD-L1 expression is associated with better disease-free survival in triple-negative breast cancer. Am J Clin Pathol 2016;146:496–502.
11. Samanta D, Park Y, Ni X, Li H, Zahnow CA, Gabrielson E, et al. Chemotherapy induces enrichment of CD47(+)/CD73(+)/PDL1(+) immune evasive triple-negative breast cancer cells. Proc Natl Acad Sci U S A 2018;115:E1239–E48.
12. Black M, Barsoum IB, Truesdell P, Cotechini T, Macdonald-Goodfellow SK, Petroff M, et al. Activation of the PD-1/PD-L1 immune checkpoint confers tumor cell chemoresistance associated with increased metastasis. Oncotarget 2016;7:10557–67.
13. Chang CH, Qiu J, O'Sullivan D, Buck MD, Noguchi T, Curtis JD, et al. Metabolic competition in the tumor microenvironment is a driver of cancer progression. Cell 2015;162:1229–41.
14. Clark CA, Gupta HB, Sareddy G, Pandeswara S, Lao S, Yuan B, et al. Tumor-intrinsic PD-L1 signals regulate cell growth, pathogenesis, and autophagy in ovarian cancer and melanoma. Cancer Res 2016;76:6964–74.
15. Chen N, Fang W, Lin Z, Peng P, Wang J, Zhan J, et al. KRAS mutation-induced upregulation of PD-L1 mediates immune escape in human lung adenocarcinoma. Cancer Immunol Immunother 2017;66:1175–87.
16. Garon EB, Rizvi NA, Hui R, Leighl N, Balmanoukian AS, Eder JP, et al. Pembrolizumab for the treatment of non-small-cell lung cancer. N Engl J Med 2015;372:2018–28.
17. Coelho MA, de Carne Trecesson S, Rana S, Zecchin D, Moore C, Molina-Arcas M, et al. Oncogenic RAS signaling promotes tumor immunoresistance by stabilizing PD-L1 mRNA. Immunity 2017;47:1083–99.
18. D'Incecco A, Andreozzi M, Ludovini V, Rossi E, Capodanno A, Landi L, et al. PD-1 and PD-L1 expression in molecularly selected non-small-cell lung cancer patients. Br J Cancer 2015;112:95–102.
19. Ji M, Liu Y, Li Q, Li X, Ning Z, Zhao W, et al. PD-1/PD-L1 expression in non-small-cell lung cancer and its correlation with EGFR/KRAS mutations. Cancer Biol Ther 2016;17:407–13.
20. Lastwika KJ, Wilson W 3rd, Li QK, Norris J, Xu H, Ghazarian SR, et al. Control of PD-L1 expression by oncogenic activation of the AKT-mTOR pathway in non-small cell lung cancer. Cancer Res 2016;76:227–38.
21. Jiang X, Zhou J, Giobbie-Hurder A, Wargo J, Hodi FS. The activation of MAPK in melanoma cells resistant to BRAF inhibition promotes PD-L1 expression that is reversible by MEK and PI3K inhibition. Clin Cancer Res 2013;19:598–609.
22. Mittendorf EA, Philips AV, Meric-Bernstam F, Qiao N, Wu Y, Harrington S, et al. PD-L1 expression in triple-negative breast cancer. Cancer Immunol Res 2014;2:361–70.
23. Noman MZ, Desantis G, Janji B, Hasmim M, Karray S, Dessen P, et al. PD-L1 is a novel direct target of HIF-1alpha, and its blockade under hypoxia enhanced MDSC-mediated T cell activation. J Exp Med 2014;211:781–90.
24. Lee SJ, Jang BC, Lee SW, Yang YI, Suh SI, Park YM, et al. Interferon regulatory factor-1 is prerequisite to the constitutive expression and IFN-gamma-induced upregulation of B7-H1 (CD274). FEBS Lett 2006;580:755–62.
25. Loke P, Allison JP.PD-L1 and PD-L2 are differentially regulated by Th1 and Th2 cells. Proc Natl Acad Sci U S A 2003;100:5336–41.
26. Gowrishankar K, Gunatilake D, Gallagher SJ, Tiffen J, Rizos H, Hersey P. Inducible but not constitutive expression of PD-L1 in human melanoma cells is dependent on activation of NF-kappaB. PLoS One 2015;10:e0123410.
27. Mezzadra R, Sun C, Jae LT, Gomez-Eerland R, de Vries E, Wu W, et al. Identification of CMTM6 and CMTM4 as PD-L1 protein regulators. Nature 2017;549:106–10.
28. Burr ML, Sparbier CE, Chan YC, Williamson JC, Woods K, Beavis PA, et al. CMTM6 maintains the expression of PD-L1 and regulates anti-tumour immunity. Nature 2017;549:101–5.
29. Li CW, Lim SO, Xia W, Lee HH, Chan LC, Kuo CW, et al. Glycosylation and stabilization of programmed death ligand-1 suppresses T-cell activity. Nat Commun 2016;7:12632.
30. Yang Y, Hsu JM, Sun L, Chan LC, Li CW, Hsu JL, et al. Palmitoylation stabilizes PD-L1 to promote breast tumor growth. Cell Res 2019;29:83–6.
31. Li CW, Lim SO, Chung EM, Kim YS, Park AH, Yao J, et al. Eradication of triple-negative breast cancer cells by targeting glycosylated PD-L1. Cancer Cell 2018;33:187–201.
32. Sun C, Wang L, Huang S, Heynen GJ, Prahallad A, Robert C, et al. Reversible and adaptive resistance to BRAF(V600E) inhibition in melanoma. Nature 2014;508:118–22.
33. Li W, Xu H, Xiao T, Cong L, Love MI, Zhang F, et al. MAGeCK enables robust identification of essential genes from genome-scale CRISPR/Cas9 knockout screens. Genome Biol 2014;15:554.
34. Rhie SK, Hazelett DJ, Coetzee SG, Yan C, Noushmehr H, Coetzee GA. Nucleosome positioning and histone modifications define relationships between regulatory elements and nearby gene expression in breast epithelial cells. BMC Genomics 2014;15:331.
35. Wang Y, Zhang T, Kwiatkowski N, Abraham BJ, Lee TI, Xie S, et al. CDK7-dependent transcriptional addiction in triple-negative breast cancer. Cell 2015;163:174–86.
36. Abraham BJ, Hnisz D, Weintraub AS, Kwiatkowski N, Li CH, Li Z, et al. Small genomic insertions form enhancers that misregulate oncogenes. Nat Commun 2017;8:14385.
37. Davis CA, Hitz BC, Sloan CA, Chan ET, Davidson JM, Gabdank I, et al. The encyclopedia of DNA elements (ENCODE): data portal update. Nucleic Acids Res 2018;46:D794–801.
38. Gertz J, Savic D, Varley KE, Partridge EC, Safi A, Jain P, et al. Distinct properties of cell-type-specific and shared transcription factor binding sites. Mol Cell 2013;52:25–36.
39. Barretina J, Caponigro G, Stransky N, Venkatesan K, Margolin AA, Kim S, et al. The cancer cell line encyclopedia enables predictive modelling of anticancer drug sensitivity. Nature 2012;483:603–7.
40. Cancer Genome Atlas N. Comprehensive molecular portraits of human breast tumours. Nature 2012;490:61–70.
41. Cancer Genome Atlas Research N. Comprehensive molecular profiling of lung adenocarcinoma. Nature 2014;511:543–50.
42. Love MI, Huber W, Anders S. Moderated estimation of fold change and dispersion for RNA-seq data with DESeq2. Genome Biol 2014;15:550.
43. Tofigh A, Suderman M, Paquet ER, Livingstone J, Bertos N, Saleh SM, et al. The prognostic ease and difficulty of invasive breast carcinoma. Cell Rep 2014;9:129–42.
44. Varley KE, Gertz J, Roberts BS, Davis NS, Bowling KM, Kirby MK, et al. Recurrent read-through fusion transcripts in breast cancer. Breast Cancer Res Treat 2014;146:287–97.
45. Seo JS, Ju YS, Lee WC, Shin JY, Lee JK, Bleazard T, et al. The transcriptional landscape and mutational profile of lung adenocarcinoma. Genome Res 2012;22:2109–19.
46. Djureinovic D, Hallstrom BM, Horie M, Mattsson JS, La Fleur L, Fagerberg L, et al. Profiling cancer testis antigens in non-small-cell lung cancer. JCI Insight 2016;1:e86837.
47. Prat A, Navarro A, Pare L, Reguart N, Galvan P, Pascual T, et al. Immune-related gene expression profiling after PD-1 blockade in non-small cell lung carcinoma, head and neck squamous cell carcinoma, and melanoma. Cancer Res 2017;77:3540–50.
48. Almozyan S, Colak D, Mansour F, Alaiya A, Al-Harazi O, Qattan A, et al. PD-L1 promotes OCT4 and nanog expression in breast cancer stem cells by sustaining PI3K/AKT pathway activation. Int J Cancer 2017;141:1402–12.
49. Ponta H, Sherman L, Herrlich PA. CD44: from adhesion molecules to signalling regulators. Nat Rev Mol Cell Biol 2003;4:33–45.
50. Jaggupilli A, Elkord E.Significance of CD44 and CD24 as cancer stem cell markers: an enduring ambiguity. Clin Dev Immunol 2012;2012:708036.
51. Okamoto I, Kawano Y, Murakami D, Sasayama T, Araki N, Miki T, et al. Proteolytic release of CD44 intracellular domain and its role in the CD44 signaling pathway. J Cell Biol 2001;155:755–62.
52. Thorne RF, Legg JW, Isacke CM. The role of the CD44 transmembrane and cytoplasmic domains in co-ordinating adhesive and signalling events. J Cell Sci 2004;117:373–80.
53. Cho Y, Lee HW, Kang HG, Kim HY, Kim SJ, Chun KH. Cleaved CD44 intracellular domain supports activation of stemness factors and promotes tumorigenesis of breast cancer. Oncotarget 2015;6:8709–21.
54. Miletti-Gonzalez KE, Murphy K, Kumaran MN, Ravindranath AK, Wernyj RP, Kaur S, et al. Identification of function for CD44 intracytoplasmic domain (CD44-ICD): modulation of matrix metalloproteinase 9 (MMP-9) transcription via novel promoter response element. J Biol Chem 2012;287:18995–9007.
55. Sugahara KN, Murai T, Nishinakamura H, Kawashima H, Saya H, Miyasaka M. Hyaluronan oligosaccharides induce CD44 cleavage and promote cell migration in CD44-expressing tumor cells. J Biol Chem 2003;278:32259–65.

56. De Falco V, Tamburrino A, Ventre S, Castellone MD, Malek M, Manie SN, et al. CD44 proteolysis increases CREB phosphorylation and sustains proliferation of thyroid cancer cells. Cancer Res 2012;72:1449–58.
57. Sumimoto H, Takano A, Teramoto K, Daigo Y. RAS-mitogen-activated protein kinase signal is required for enhanced PD-L1 expression in human lung cancers. PLoS One 2016;11:e0166626.
58. Cerami E, Gao J, Dogrusoz U, Gross BE, Sumer SO, Aksoy BA, et al. The cBio cancer genomics portal: an open platform for exploring multidimensional cancer genomics data. Cancer Discov 2012;2:401–4.
59. Zhang G, Guo L, Yang C, Liu Y, He Y, Du Y, et al. A novel role of breast cancer-derived hyaluronan on inducement of M2-like tumor-associated macrophages formation. Oncoimmunology 2016;5:e1172154.
60. Shipitsin M, Campbell LL, Argani P, Weremowicz S, Bloushtain-Qimron N, Yao J, et al. Molecular definition of breast tumor heterogeneity. Cancer Cell 2007;11:259–73.
61. Nishino M, Ozaki M, Hegab AE, Hamamoto J, Kagawa S, Arai D, et al. Variant CD44 expression is enriching for a cell population with cancer stem cell-like characteristics in human lung adenocarcinoma. J Cancer 2017;8:1774–85.
62. Lee Y, Shin JH, Longmire M, Wang H, Kohrt HE, Chang HY, et al. CD44+ cells in head and neck squamous cell carcinoma suppress T-cell-mediated immunity by selective constitutive and inducible expression of PD-L1. Clin Cancer Res 2016;22:3571–81.
63. Castagnoli L, Cancila V, Cordoba-Romero SL, Faraci S, Talarico G, Belmonte B, et al. WNT signaling modulates PD-L1 expression in the stem cell compartment of triple-negative breast cancer. Oncogene 2019;38:4047–60.
64. Alsuliman A, Colak D, Al-Harazi O, Fitwi H, Tulbah A, Al-Tweigeri T, et al. Bidirectional crosstalk between PD-L1 expression and epithelial to mesenchymal transition: significance in claudin-low breast cancer cells. Mol Cancer 2015;14:149.
65. Menke-van der Houven van Oordt CW, Gomez-Roca C, van Herpen C, Coveler AL, Mahalingam D, Verheul HM, et al. First-in-human phase I clinical trial of RG7356, an anti-CD44 humanized antibody, in patients with advanced, CD44-expressing solid tumors. Oncotarget 2016;7:80046–58.